Improved Experimental Agreement of Ionization and Pressure Peak Location by Adding a Dynamical NO-Model

Master's thesis
performed in **Vehicular Systems**

by
Daniel Claesson

Reg nr: LiTH-ISY-EX-3554-2004

25th May 2004

Improved Experimental Agreement of Ionization and Pressure Peak Location by Adding a Dynamical NO-Model

Master's thesis

performed in **Vehicular Systems**,
Dept. of Electrical Engineering
at **Linköpings universitet**

by **Daniel Claesson**

Reg nr: LiTH-ISY-EX-3554-2004

Supervisor: **Gunnar Cedersund**
          Linköpings Universitet

Examiner: **Associate Professor Lars Eriksson**
          Linköpings Universitet

Linköping, 25th May 2004

Avdelning, Institution Division, Department Vehicular Systems, Dept. of Electrical Engineering 581 83 Linköping			**Datum** Date 25th May 2004

Titel	Förbättrad experimentell överenstämmelse med jonström- och tryck-toppsläge genom införande av en dynamisk NO-modell
Title	Improved Experimental Agreement of Ionization and Pressure Peak Location by Adding a Dynamical NO-Model

Författare Daniel Claesson
Author

Sammanfattning
Abstract

Modelling combustion engines is an important tool in engine research. Development and modelling of ionization current has potential in developing virtual pressure sensors based on ionization measurements. Previous models has problem when predicting the true relationship between the pressure peak location and ionization peak location, and both too early and too late predictions has been observed. An explanation for these discrepancies are provided and a model where the experimental mismatch has been reduced to less than one CAD is also presented. This is well within the measurement uncertainty.

Abstract

Modelling combustion engines is an important tool in engine research. Development and modelling of ionization current has potential in developing virtual pressure sensors based on ionization measurements. Previous models has problem when predicting the true relationship between the pressure peak location and ionization peak location, and both too early and too late predictions has been observed. An explanation for these discrepancies are provided and a model where the experimental mismatch has been reduced to less than one CAD is also presented. This is well within the measurement uncertainty.

Keywords: zonal models, combustion, ionization current, experimental verification, sensitivity analysis, dynamical NO-models

Preface

This thesis was performed in Vehicular Systems, Department of Electrical Engineering at Linköpings Universitet, during the autumn 2003 and spring 2004. The report is written using LaTeX.

Thesis Outline

The first chapter gives a short introduction to the area combustion modelling and ionization currents. The following chapter treats the basic Otto motor concept and the multi-zonal model. Here, the theory behind ionization current and different NO-models are explained. The third chapter deals with the methods used when implementing the dynamical NO-model. The main work has been done in the fourth chapter, which consists of the results and analysis from various simulations. The last chapter discuss the conclusions of the work and some points for future work.

Acknowledgment

Firstly I would like to thank my supervisor Gunnar Cedersund for all his ideas and discussions and my examiner Lars Eriksson. I would also like to thank Jan Åslund for the mathematics behind the 3-dimensional spline interpolation. Not forgetting my friends in the final thesis room, Johanna Wallén and Otto Montell. At last I would like to give my appreciations to the staff at Vehicular Systems.

Contents

x

Chapter 1

Introduction

1.1 Why Model Combustion Engines?

Simulating combustion engines is an important tool in research and development of new engine concepts. With the increasing computer capacity it will in the future be possible to do real time in-car combustion simulations. Given good models, this will provide engine management systems useful information. Considering the time needed to get good models, it is important to already now develop them.

1.2 Why do Combustion Models?

The simplest models developed considers the whole cylinder as one zero-dimensional zone. Zero-dimensional means that there is no spatial variations within the zone. In the one-zone models this means that the temperature and the pressure is uniform throughout the cylinder. A more advanced model is the two-zone zero-dimensional model, where we have one burned and one unburned zone. Here each zone has its own temperature and chemical composition and the pressure is uniform in the whole cylinder.

In order to estimate thermal stresses on engine parts and to calculate the number of ionized particles a higher resolution of the temperature gradients within the cylinder is needed. To get this a theoretical multi-zone zero-dimensional model has been developed at Vehicular System, ISY, LiTH [8]. A Java implementation of the model has been developed by Johan Gill, Gunnar Cedersund and Karl-Johan Nogenmyr in [6, 9].

1.3   Why Model Ionization Currents?

One simple way to monitor the combustion online is ionization current sensing. This is done by applying a voltage across the spark plug and measurement of the current that flows through. The in-cylinder free ions and their electrons will conduct the current. By modeling the ionization current, and comparing it with experiments, the physics behind, that not yet is fully understood, can be revealed. When this is done, the engine management systems can use the real time measured ionization current to control the engine by, for example, prediction of the position of the pressure peak.

1.4   The Current Situation

When starting to work on this thesis there were some tasks to deal with. The first was the results Ingemar Andersson did in his lic, [2]. These results showed that the simulated ionization current peak position was located about 2 CAD[1] later than the measured peak position. In his simulations he did not use any kind of heat transfer, massflow between zones or a multi-zonal model. A plot of Andersson's results can be seen in Figure 1.1.

The second was the results Karl-Johan Nogenmyr did in his master thesis [9]. In Nogenmyr's simulations the ionization current peak positions was located about 4 CAD earlier than the measured peak position. Nogenmyr used different heat transfer models and a multi-zonal combustion model. He also included massflow between the zones. In Figure 1.2 three simulations with different heat transfer models are done.

1.5   Objectives of this Thesis

The objectives of this thesis can be summarized in three parts

1. To state if the observation that the simulated ionization current peak, always is a few degrees earlier than the measured peak is correct. This is done by model validation in three parts

   - Redoing the experimental verification done at the end of Karl-Johans master thesis.
   - Extending the verification with more data.
   - Sensitivity analysis with respect to all parameters that are not considered as cycle-to-cycle specific.

---

[1]Crank angle degrees
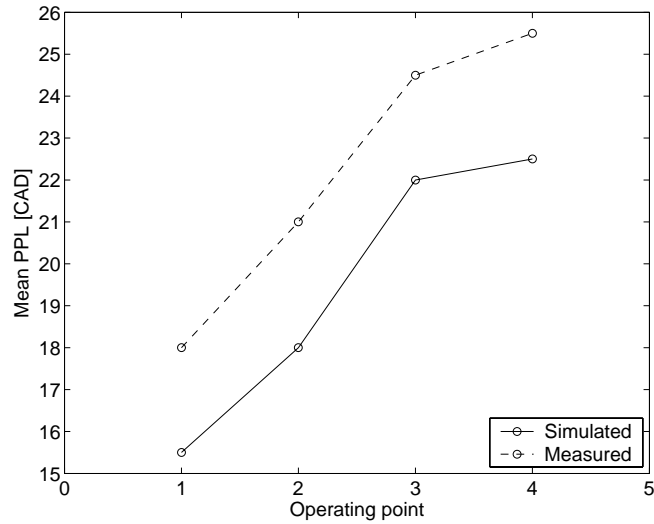
Figure 1.1: *Pressure peak location for four different operating points. The simulations was done without any heat transfer model. The difference of about 2 CAD between simulated and measured pressure peak location can directly be translated to ionization current peak location. This 2 CAD delay was one of the conclusions in Andersson's Lic. [2, Fig. 6.5(a)].*
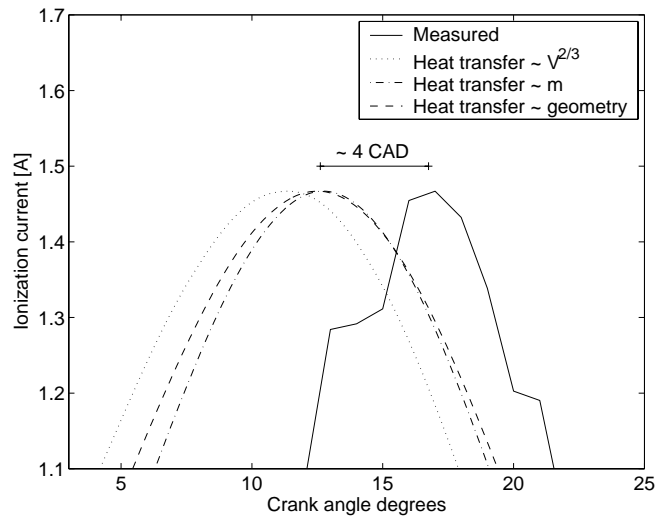
Figure 1.2: *Simulations done with three different heat transfer models. The simulated ionization current peak location is about 4 CAD earlier than the measured peak location.*
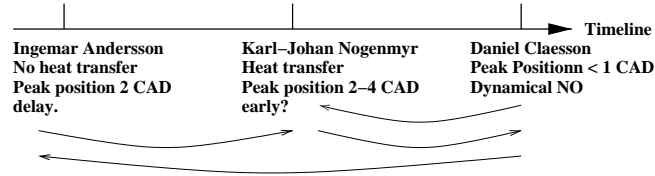
Figure 1.3: *Project time-line.*
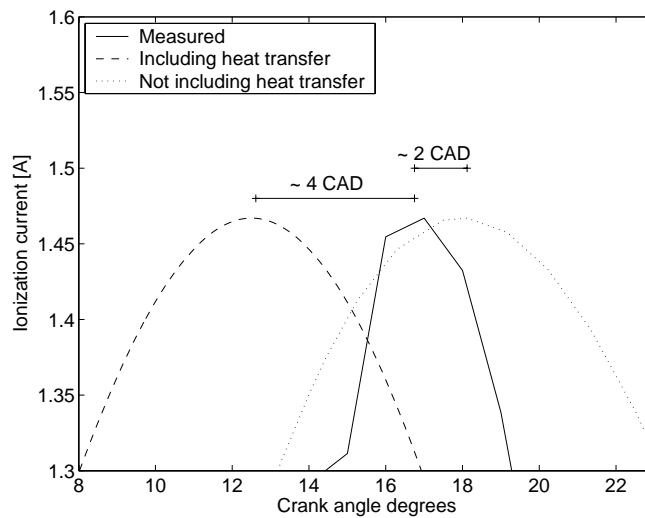
Figure 1.4: *Ionization current plots. One using a heat transfer model, one without any heat transfer. The measured ionization current is also plotted.*

2. To explain the difference between Karl-Johan Nogenmyr's [9] and Ingemar Andersson's [2] results. In Figure 1.4 the difference between Andersson's simulations without heat transfer and Nogenmyr's with heat transfer.

3. To state whether the difference between the simulated ionization current peak and measured peak, can be decreased, by for example adding a dynamical NO-model.

Chapter 2

Theory

This chapter is divided into four parts. The first part is a short introduction to the four-stroke Otto engine. Part two deals with one of several models describing combustion/compression in a cylinder. The two last parts is about ionization current models and NO-models, respectively.

2.1 Short Four-stroke Otto Engine Concepts

The four-stroke Otto enigne is a machine that converts chemical energy in the fuel into mechanical energy and heat. As the name implies it operates in four stages, see Figure 2.1. In the first stage (a) the piston is moving downwards as the intake valve is open. The fuel, typically air mixed with gasoline, flows into the cylinder due to the pressure difference in the intake manifold and the cylinder, caused by the movement of the piston. When the piston reaches its lower turning point the intake valve closes, and as the piston moves up (b) it compresses the fuel. When it reaches a certain point, (the ignition angle) before its upper turning point an electric circuit creates a spark in the gap between the spark plugs two electrodes. This starts the combustion. While the combustion occurs the piston turns at its upper turning point. During the expansion phase the piston moves downward (c) and some of the internal energy of the combusted gas is converted to mechanical energy. When the piston reaches its lower turning point the exhaust valve opens and as the piston moves up (d) the now combusted gas flows out in the exhaust pipe.

When modeling the Otto engine, many equation are written as a function of the position of the crank. The most common notation is the angle between the crank and the axis of the cylinder, see Figure 2.2.
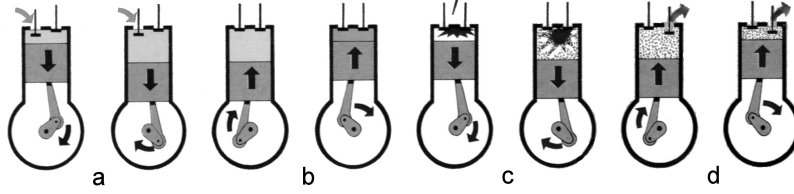
Figure 2.1: *The four-stroke Otto cycle.*
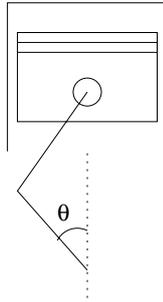
Figure 2.2: *The angle θ determines the position of the piston*

2.2 Combustion/Compression Models

There exists several combustion/compression models. The one used is
explained in this section.

   During the simulation, the cylinder is divided into an arbitrary num-
ber of zones. First, during the compression, there is only one unburned
zone. As the combustion starts a new small burned zone is created and
a mass-flow from the unburned zone to the burned zone is established.
When the zone reaches a certain mass limit its mass-flow is cut off, and
a new small zone is created between the two zones. The mass-flow from
the unburned zone continues to flow but now to the new zone. When
this new zone reaches the mass limit its mass-flow is also cut off, and
a new zone is created. This process continues until all the mass in the
unburned zone is consumed. The mass-flow between the unburned and
the burned zone is determined by the experimental Vibe function:

$$x_b(\theta) = \frac{m_b}{m_{tot}} = 1 - e^{-a(\frac{\theta-\theta_0}{\Delta\theta})^{m+1}} . \tag{2.1}$$

This determines the mass fraction burned x_b, the ratio between the
burned mass, m_b and the total mass m_{tot}, as a function of the crank
angle θ. Here θ_0 is the angle at which the combustion starts, $\Delta\theta$ is
the combustion duration. a and m are adjustable parameters. This is,
as already said, an experimentally developed function, and there are

alternatives. One is to calculate the instantaneous burn rate by flame speed times flame area, see [10, 11].

2.2.1 Derivation of the Multi Zonal Model

As said before the in-cylinder pressure is assumed to be spatially invariant. What remains to be unique for the zones are their temperatures, volumes and chemical composition. Two assumptions are made.

- The reactions in a burned zone are fast enough, to be aprroximated as in equilibrium.

- The reactions in the unburned zone are slow enough, to be approximated as frozen.

The first relation to be satisfied is the balance equation for the volumes:

$$dV = \sum_i dV_i \; , \tag{2.2}$$

where dV_i is the change of volume for zone i, and dV is the change of volume for the whole system, typically due to movement of the piston. For each zone the ideal gas law, $pV = mRT$, must be satisfied, in the differentiated form:

$$V_i dp + p dV_i = R_i T_i dm_i + m_i T_i dR_i + m_i R_i dT_i \; . \tag{2.3}$$

An energy conservation equation to be satisfied for all zones:

$$dU = dW + dQ \; . \tag{2.4}$$

Equation (2.2), (2.3) and (2.4) forms a system with $2N+1$ ODE's[1]. These ODE's are highly non-linear but can be put in a matrix form as follows:

$$\mathbf{A} d\mathbf{x} = \mathbf{B} \; , \tag{2.5}$$

where $d\mathbf{x}$ is the change in the system:

$$d\mathbf{x} = [dp \; dV_1 \; dT_1 \; \ldots \; dV_N \; dT_N]^T \; . \tag{2.6}$$

The $\mathbf{A}$ and $\mathbf{B}$ matrices are as following:

$$\mathbf{A} = \begin{pmatrix} 0 & 1 & 0 & \ldots & 1 & 0 \\ a_1 & p & b_1 & \ldots & 0 & 0 \\ c_1 & p & d_1 & \ldots & 0 & 0 \\ \vdots & \vdots & \vdots & \ddots & \vdots & \vdots \\ a_N & 0 & 0 & \ldots & p & b_N \\ c_N & 0 & 0 & \ldots & p & d_N \end{pmatrix} \; ,$$

---

[1]Ordinary Differential Equation

$$\mathbf{B} = \begin{pmatrix} dV \\ R_i T_i \sum_{i \neq 1} dm_{1i} \\ \delta Q_1 + \sum_{i \neq 1}(h_{1i} - h_1 + R_1 T_1)dm_{1i} \\ \vdots \\ R_N T_N \sum_{i \neq N} dm_{Ni} \\ \delta Q_N + \sum_{i \neq N}(h_{Ni} - h_N + R_N T_N)dm_{Ni} \end{pmatrix} .$$

The a_i, b_i, c_i and d_i coefficients in the $\mathbf{A}$ matrix are:

$$a_i = V_i\left(1 - \frac{p}{R_i}\left(\frac{\partial R_i}{\partial p}\right)_{T_i}\right) \tag{2.7}$$

$$b_i = -m_i\left(R_i + T_i\left(\frac{\partial R_i}{\partial T_i}\right)_p\right) \tag{2.8}$$

$$c_i = -m_i T_i\left(\frac{T_i}{p}\left(\frac{\partial R_i}{\partial T_i}\right)_p + \left(\frac{\partial R_i}{\partial p}\right)_{T_i}\right) \tag{2.9}$$

$$d_i = m_i\left(c_p - R_i - T_i\left(\frac{\partial R_i}{\partial T_i}\right)_p\right) . \tag{2.10}$$

When equation (2.5) is solved for $d\mathbf{x}$, one gets the change in the system as a function of the present state. By this a numerical integrator can calculate the next state. A more detailed study of the calculations has been made by Eriksson [3].

2.2.2   Initial Temperature of a Burned Zone

When a new burned zone is created it must have a correct initial temperature, T_{b_i}. This temperature can be found by solving

$$h_u(T_u, p) = h_b(T_b, p) , \tag{2.11}$$

i.e. the enthalpy for the combusted mass, h_b is the same as the enthalpy for the uncombusted mass, h_u. In the Java implementation these enthalpies are tabulated in a table generated with CHEPP [4]. A detailed description is available in [3].

2.2.3   Heat Transfer

Since there is a temperature difference, ΔT, between the in-cylinder gas and the cylinder walls, we have included an energy flow. According to Newton's law of cooling, the heat transmitted through the gas-cylinder contact area A per unit time is:

$$\frac{dQ}{dt} = hA\Delta T . \tag{2.12}$$

B	9.0e-2 [m]
C_1	2 [ ]
p	[Pa]
p_f	[Pa]
p_m	[Pa]
T_{IVC}	363 [K]
V_{disp}	4.94e-4 [m^3]
C_2	0.44 [ ]
p_{IVC}	6.5e4 [Pa]
V_{IVC}	[m^3]
U_p	4.97 [m/s]
T	[K]

Table 2.1: *Parameter list for the heat transfer model.*

In equation (2.13), p_f is the pressure in a firing cycle and p_m is the pressure in a motored cycle, a cycle without combustion. C_1 and C_2 are motor-type dependent constants. U_p is the mean velocity of the piston. This gives the heat transfer coefficient used in the simulations, see [12]:

$$h = \frac{253 B^{-0.2} C_1 p^{0.8} \left(\frac{0.0034 (p_f - p_m) T_{IVC} V_{disp} C_2}{p_{IVC} V_{IVC}} + U_p \right)^{0.8}}{T^{0.53}} \qquad (2.13)$$

All the parameters and their values in equation (2.13) are tabulated in Table 2.1.

2.3   Ionization Current Models

As the combustion occurs some of the nitrogen in the air is oxidized into NO, typically around one percent. Due to the high temperature within the cylinder this NO is thermally ionized into NO^+. The presence of these ions and their free electrons can be detected by applying a voltage across the spark plug electrodes. Technology and theory for this topic has been developed at Vehicular Systems the recent years, and several publications has been written. A detailed study of the research has been put together by Andersson [2].

The current that flows through the spark plug has a characteristic shape in the time domain, with one peak around TDC[2], and one peak 10 to 15 CAD after TDC. The second peak may be caused by the ionized NO and it has also a strong correlation to the cylinder pressure peak. This makes the ionization current an interesting property for real time

---

[2]Top Dead Center. i.e. the piston is at its upper position.
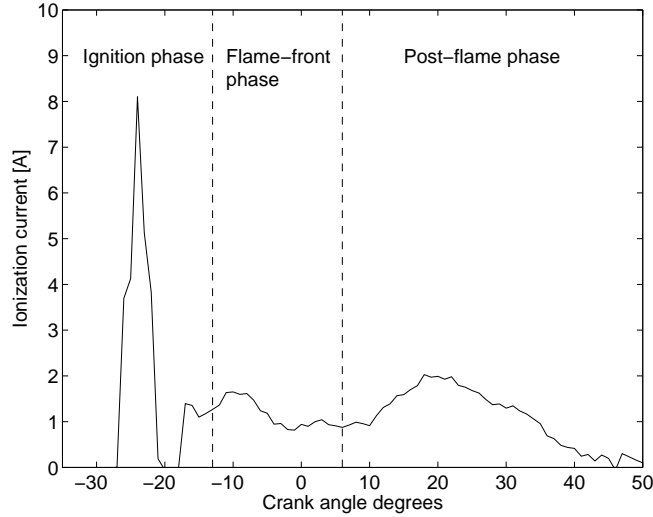
Figure 2.3: *Example of a measured ionization current with its three characteristic phases.*

monitoring of the combustion when cylinder pressure is not directly measured. There exists several different ionization current models, and some of them are presented in the next part.

2.3.1 Saitzkoff-Reinmann Model

Saitzkoff et al. [1] has made an approach, based on thermal ionization of NO, to explain the second peak. A cylinder shaped control volume is put between the spark plug electrodes, see Figure 2.4. Since the electric field is strongest here, the ions and the free electrons in this cylinder will make the main contribution to the conduction. The free electrons are highly mobile compared to the ions and these will dominate the current. Saha has put up an equation for thermally generated free electrons (see [1] for assumptions) that describes the balance of the ion and electron concentration when first order ionization is considered:

$$\frac{n_1 n_e}{n_0} = 2\left(\frac{2\pi m_e kT}{h^2}\right)^{\frac{3}{2}} \frac{B_1}{B_0} e^{-\frac{E_1}{kT}} \ . \qquad (2.14)$$
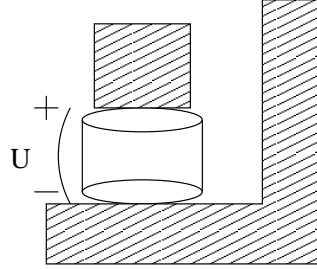
Figure 2.4: *The spark plugs two electrodes with the voltage U applied. The cylinder shaped volume contains the ions and the free electrons conducting the current.*

This equation combined with electron drift velocity gives the current I when the voltage U is applied:

$$I = U \frac{\pi r^2}{d} \frac{e^2}{\sigma m_e \sqrt{\frac{8kT}{\pi m_e}}} \sqrt{\phi_s} \sqrt{\frac{2\left(\frac{2\pi m_e kT}{h^2}\right)^{\frac{3}{2}} \frac{B_1}{B_0} e^{-\frac{E_1}{kT}}}{n_{tot}}} \qquad (2.15)$$

$$\phi_s = \frac{[NO] \cdot 10^6}{n_{tot}/N_A} \qquad (2.16)$$

$$n_{tot} = \frac{p}{\tilde{R}T_k} N_A \ . \qquad (2.17)$$

All entries in these equations are found in Table 2.2.

2.3.2 Calcote Model

This model was presented by Calcote 1963. In the Calcote model the spark plug is modeled as a Langmuir probe. The central electrode has some electrical potential, U_s relative the grounded parts of the spark plug. In the combustion chamber there is a mixture of ionized gases, including positive and negative ions and free electrons. If the electrical potential U_s is negative enough all electrons will be repelled by the electrical field. Only the positive ions will produce some current. If U_s increase towards positive the fastest electrons will start to overcome the electrical field and produce some current.

The surface process at the electrodes can be described with the

n_1	Number density of ions [ ]	T	Temperature of gas [K]
n_e	Number density of free electrons [ ]	ϕ_s	Ratio of NO in gas mixture [ ]
n_0	Number density of neutral particles [ ]	m_e	Electron mass [kg]
U	Measurement voltage [V]	B_i	Internal partition function
r	Radius of measurement cylinder [m]	E_1	Ionization energy for 1st order ionization [J]
d	Length of measurement cylinder [m]	n_{tot}	Total particle density density [1/m^3]
σ	Collision cross section [m^2]	k	Boltzmann's constant [J/K]
$[NO]$	NO Concentration [mol/cm^3]	h	Planck's constant [Js]
$\tilde{R}$	Universal gas constant [ ]	e	Unit charge constant [As]
T_k	Kernel temperature [K]	N_A	Avogadro constant [molecule/mol]
p	Cylinder pressure [Pa]		

Table 2.2: *Parameter list for the Saitzkoff-Reinmann equation.*

U	80 [V]
r	1 [mm]
d	1 [mm]
σ	0.1 [Å^2]
m_e	9.31×10^{-31} [kg]
$\frac{B_1}{B_0}$	1 [ ]
E_1	9.25 [eV]
k	1.38×10^{-23} [J/K]
h	6.63×10^{-34} [Js]
e	1.6×10^{-19} [As]

Table 2.3: *Parameter values in Saitzkoff-Reinmann model.*

n_e	Electron concentration [ ]	X_e	$= l + 2\lambda_e$ [m]
m_e	Electron mass [kg]	B_e	$= \sqrt{X_e^2 - (d + 2\lambda_e)^2}$ [m]
T_e	Electron temperature [K]	n_i	Ion concentration [ ]
λ_e	Electron mean free path [m]	m_i	Ion mass [kg]
e	Unit charge [As]	T_i	Ion temperature [K]
l	Probe length [m]	λ_i	Ion mean free path [m]
d	Probe diameter [m]	X_i	$= l + 2\lambda_i$ [m]
A_s	Probe surface area [m^3]	B_i	$= \sqrt{X_i^2 - (d + 2\lambda_i)^2}$ [m]

Table 2.4: *Parameter list for the Calcote model*

following expressions:

$$I_e = n_e e A_s \sqrt{\frac{kT_e}{2\pi m_e}} \left[1 + \frac{3ld}{16\lambda_e B_e} \ln\left(\frac{X_e + B_e}{X_e - B_e} \right) \right]^{-1} \qquad (2.18)$$

$$I_e = n_i e A_s \sqrt{\frac{kT_i}{2\pi m_i}} \left[1 + \frac{3ld}{16\lambda_i B_i} \ln\left(\frac{X_i + B_i}{X_i - B_i} \right) \right]^{-1}, \qquad (2.19)$$

where all entries are listed in Table 2.4. The first equation is valid for electrons at the positive electrode and the second is valid for positive ions at the negative electrode.

2.3.3 Yoshiyama-Tomita Model

The theory is based on flame front ionization. Experiments were made in a combustion bomb. The combustion bomb wall can be electrically isolated or connected to one of the electrodes. The result shows to characteristic ionization current peaks. The first peak appears when the flame front is close to the spark gap. The second peak only appear when the bomb wall is connected to the negative electrode, and when the flame front reaches the wall. Two conclusions were drawn from the experiments:

- The ionization current shape is dependent of the flame position and electrode polarity.

- Ions and electrons are generated in the flame front by chemical reactions and thermal ionization is negligible.

A more extensive explanation of the Calcote model and the Yoshiyama-Tomita model can be found in [2].

There are a number of ways of calculating the NO-concentration. This is the topic of the next section.

2.4 NO-Models

2.4.1 Fix NO Concentration

The fixed NO concentration model used in earlier simulations uses a fixed value on the Φ_s parameter, typically 0.01. This means that one percent of the gas mixture in the cylinder consists of NO.

The simulations done by Karl-Johan Nogenmyr in [9] showed that with a fixed NO concentration, the simulated ionization current peak is a few CAD earlier than the measured peak.

2.4.2 Dynamical NO Concentration

The core in the dynamical NO model is thermal ionization of nitric oxide, NO. The model is built up by two processes, NO formation and thermal ionization. Most reactions, except for NO formation, are described as fast compared to the time-scale of a combustion and the concentrations are close to equilibrium. The formation of NO is slower and is better described as reaction rate limited rather than in equilibrium.

In [2] exists a more detailed description of the mechanism behind NO formation and thermal ionization. In the following part only the fundamental mechanism is described.

The description of the model does not cover the formation of all species in the reactions. These species were calculated using the Matlab program CHEPP [4]. The equilibrium concentration of NO was the compared between the Heywood model, [7] and the CHEPP program.

The dominating reactions in NO formations are:

$$O + N_2 \rightleftharpoons NO + N$$
$$N + O_2 \rightleftharpoons NO + O$$
$$N + OH \rightleftharpoons NO + H \ .$$
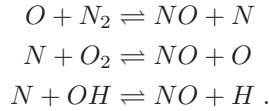
With the following two assumptions:

1. The content of N is small and changes slowly compared to the content of NO.

2. Concentrations of O, O_2, OH, H and N_2 can be approximated by their equilibrium concentrations.

The expression for NO formation is:

$$\frac{d\,[NO]}{dt} = \frac{2R_1(1 - ([NO]/[NO]_e)^2)}{1 + ([NO]/[NO]_e)R_1/(R_2 + R_3)} \ , \qquad (2.20)$$

	Rate constant $\left[\frac{cm^3}{mol \times s}\right]$
k_1^+	$7.6 \times 10^{13} e^{-38000/T}$
k_1^-	1.6×10^{13}
k_2^+	$6.4 \times 10^9 \times T e^{-3150/T}$
k_2^-	$1.5 \times 10^9 e^{-19500/T}$
k_3^+	4.1×10^{13}
k_3^-	$2.0 \times 10^{14} e^{-23650/T}$

Table 2.5: *Reaction rate constants for NO formation.*

where

$$R_1 = k_1^+[O]_e[N_2]_e = k_1^-[NO]_e[N]_e$$
$$R_2 = k_2^+[N]_e[O_2]_e = k_2^-[NO]_e[O]_e$$
$$R_3 = k_3^+[N]_e[OH]_e = k_3^-[NO]_e[H]_e \ .$$

The concentration $[\ ]$ is in the unit $[mol/cm^3]$ and the reaction rate constants are listed in Table 2.5. The concentration $[NO]$ is defined as

$$[NO] = \frac{N_{NO}}{V} \ , \tag{2.21}$$

where N_{NO} is the quantity of NO in $[mol]$ distributed in the volume V. If V is constant equation (2.20) can be written as

$$\frac{1}{V}\frac{d\,N_{NO}}{dt} = \frac{2R_1(1-([NO]/[NO]_e)^2)}{1+([NO]/[NO]_e)R_1/(R_2+R_3)} \ . \tag{2.22}$$

NO Formation and Volume Change

The value of the formation rate in equation (2.20) is close to zero for a frozen mixture. This fact reveals a lack in equation (2.20). If the quantity of NO is constant but the volume will increase the NO concentration will decrease. This is the case in internal combustion engines, and an extension of equation (2.20) that accounts for a change in burned zone volume, V_b is proposed:

$$\frac{d\,[NO]}{dt} = \frac{2R_1(1-([NO]/[NO]_e)^2)}{1+([NO]/[NO]_e)R_1/(R_2+R_3)} - [NO]\frac{1}{V_b}\frac{dV_b}{dt} \ . \tag{2.23}$$

An increase of the cylinder volume in equation (2.23) will increase the burned zone volume and decrease the concentration of NO in the zone. The above model is the model used in the simulations of the ionization current.

Chapter 3

Material and Methods

3.1   Numerical Solvers

The java implementation uses the Janet package to handle the matrices and the numerical integration. The implementations handles two different integrators. The first integrator is the Runge-Kutta Pair-integrator. This integrator takes smaller time steps if the problem is stiff. First it takes the time step in four steps, then it takes the same time step in five steps, which is more accurate. Then it compares the results of these two calculations, and if they differ more than a given value, the integrator assumes that the time step was too long. It then shortens the time step and redo the calculations until the difference between the four and five steps results is smaller than the given value. A more advanced integrator is Diagonally-Implicit Runge-Kutta Pair-integrator, which is an implicit integrator for solving stiff problems. Parameters for the simulators can be found in Appendix A.1.2 and A.2.

3.2   The Dynamical NO Java Implementation

To implement the dynamical NO model into the java implementation developed by Johan Gill, Gunnar Cedersund and Karl-Johan Nogenmyr in [6, 9] different cases were considered. The first case was to implement the NO model in the existing program. This approach in fact had a couple of difficulties. First to introduce an extra state representing the NO concentration in the state vector. The program requires that the states in the state vector are in the right order to function correctly. The amount of work to rewrite the program and find all the dependencies between the state vector and the program, was consid-

ered quite big compared to the amount of work writing a completely new program. The new program would only simulate the formation of dynamical NO concentration and the ionization current based on data from the existing program. This was the second approach to write a completely new program.

The new program's task was to simulate the differential equation (2.23) using the Janet simulation package. The concentration of the unknown species such as $[N_2]$, $[O_2]$, $[OH]$, $[O]$ and $[N]$ were calculated using the Matlab program CHEPP [4]. A big table was constructed with the output concentrations with corresponding T, p and ϕ values. This table was constructed using a Matlab script which generated vectors with T, p and ϕ values. These values were used as inputs to the CHEPP function `chemEqSolve(T,p)`. To use the data in the table a three dimensional interpolation program was written. The program takes arbitrary values of T, p and ϕ and returns an interpolated value of the corresponding concentration. First three normalized variables s, t and u were created using equation: (3.1).

$$\begin{pmatrix} s \\ t \\ u \end{pmatrix} = \begin{pmatrix} p \\ T \\ \phi \end{pmatrix} \bmod \begin{pmatrix} \Delta p \\ \Delta T \\ \Delta \phi \end{pmatrix} . \tag{3.1}$$

The concentration was then evaluated as a sum of basis functions weighted with the corresponding values in the table:

$$[O]_e(s,t,u) = \sum_{i=1}^{8} [O]_{e,i} \, J_i(s,t,u) . \tag{3.2}$$

The basis functions are as follows:

$$\begin{cases} J_1(s,t,u) = 1 - s - t - u + st + su + tu - stu \\ J_2(s,t,u) = J_1(s,t,1-u) \\ J_3(s,t,u) = J_1(s,1-t,u) \\ J_4(s,t,u) = J_1(s,1-t,1-u) \\ J_5(s,t,u) = J_1(1-s,t,u) \\ J_6(s,t,u) = J_1(1-s,t,1-u) \\ J_7(s,t,u) = J_1(1-s,1-t,u) \\ J_8(s,t,u) = J_1(1-s,1-t,1-u) . \end{cases} \tag{3.3}$$

Data from the three dimensional interpolation program was sent to the main program which consists of a simulation part and a model part. The model part takes care of the differential equations of concentration for each zone. It also handles the pressure, temperature and volume data reading from file. These data comes from simulations done with the earlier simulation program. The simulation output is a file with NO concentration and ionization currents for each zone.

The dynamical NO simulation starts when the first burned zone is created. The initial NO concentration for this zone was set to the equilibrium concentration. All the other zones have zero NO concentration. For each time step new values of T, p, ϕ, V and dV/dt were generated using the data from earlier simulation. These data was used to calculated the equilibrium concentration of the unknown species.

When a new burned zone starts, the initial concentration of the zone is set to the equilibrium concentration for that zone. A short tutorial for the program can be found in Appendix B.

3.3   Description of Data

The engine parameters and used measured data, come from a turbocharged 2.3 litre SAAB engine. The engine measurement was done by Mecel. Measurement data are not calibrated in amplitude, and therefore any assumptions of the absolute values are not possible.
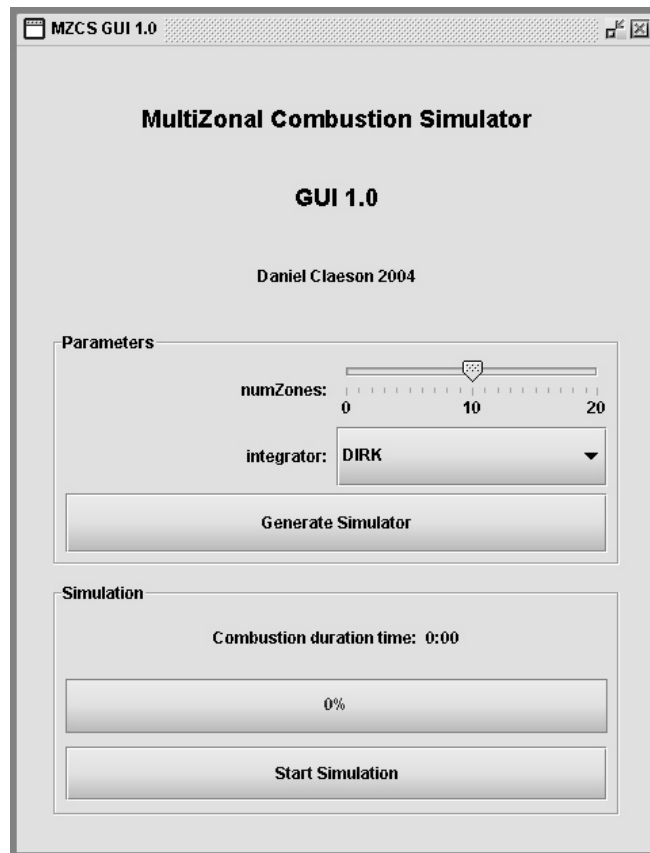
Figure 3.1: *Graphical User Interface to the Java program.*

Chapter 4

Results

As explained in the introduction the objectives of this thesis are divided into three parts. In this chapter the results of the objectives are presented.

This chapter is divided into three different parts. The first part deals with the observation that the simulated ionization current peak, always is a few CAD earlier than the measured peak [5]. A new simulation and comparison of the same data as Karl-Johan Nogenmyr did in [9] was done. Then an analysis of simulation data and measured data made with new data was done. At last a sensitivity analysis where all of the parameters was decreased and increased with several percent ended the analysis part.

The explanation of the difference between Karl-Johan Nogenmyr's and Ingemar Andersson's results is discussed in the second part. In Nogenmyr's simulations the ionization current peak position was located about 4 CAD earlier than the measured peak position. Andersson's result showed a simulated peak position 2 CAD later than the measured.

The result of all the above analysis showed that the current model did not explain all the dynamics of the ionization current. The simulated ionization current peak position was always a few CAD earlier than the measured peak position. Therefore an extended model with dynamical NO formation was considered, to decrease the difference between the simulated and measured ionization peak positions. This is what the third part is about, implementation of the dynamical NO model and evaluation and analysis of that model.
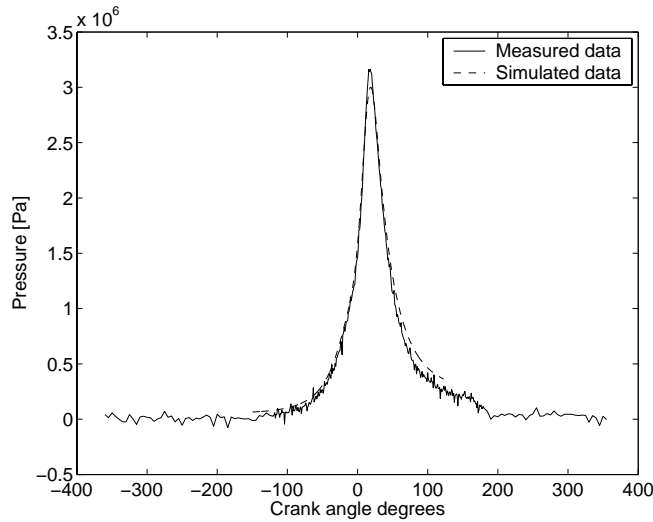
Figure 4.1: *A simulated pressure curve plotted with the measured pressure. As can be seen the curves matches quite well.*

4.1 Direct Experimental Comparison

4.1.1 New Comparison of the Same Data

To find out whether the fitting between the simulated and measured pressure is a sensitive part in the model a new comparison was done. The data used was the same as Karl-Johan Nogenmyr used in [9]. The fitting was done by adjusting the residual gas fraction, x_{res}, the combustion duration, $\Delta\theta$ in equation (2.1) and the initial temperature, T_{ivc}. The parameters were adjusted until the simulated and measured pressure curves corresponded as good as possible. To calculate the initial temperature, T_{ivc}, equation (4.1) was used. 1350 is the final temperature from a typical engine cycle, and 300 is an approximate manifold temperature:

$$T_{ivc} = 1350 * x_{res} + 300 * (1 - x_{res}) .   \quad (4.1)$$

Figure 4.1 shows a simulated pressure curve plotted with the measured pressure. The curves matches quite well, except for the amplitude.

In Table 4.1 the mean value and standard deviation of the ionization peaks position from the simulation are presented. It can be seen in Table 4.1 that the new simulation results and the old are almost identical. This means that the model is not specially sensitive in the pressure fitting. It can also be seen that the standard deviations in

θ_0 [CAD BTDC]	Comparison I		Comparison II		Measured	
	Mean	Std	Mean	Std	Mean	Std
27.0	12.36	0.27	12.44	0.39	16.00	2.14
21.1	16.19	0.52	16.03	0.71	19.45	1.64
24.1	18.26	0.40	18.26	0.48	21.65	4.15
18.1	20.74	1.28	20.05	0.85	25.25	2.75

Table 4.1: *Data from two independent simulations. The simulations have been done with different ignition angles θ_0 and the table presents the mean value and standard deviation of the ionization peak position. The first simulation was done by Karl-Johan Nogenmyr [9]. As can be seen in the table, the standard deviation in the measured values are quite big. This is a consequence of the large cycle-to-cycle variations of the ionization currents.*

the measured data are quite big. This is due to large cycle to cycle variations and even because the data is quite noisy. For each ignition angle, θ_0 eight different pressure cycles were fitted and then simulated. The eight cycles were chosen as the eight cycles where the pressure peak time occurrence was closest to the median pressure peak time occurrence.

Figure 4.2 shows a plot of the measured and simulated mean values and standard deviations for each ignition angle. The length of the lines is one standard deviation from the middle of the line were the mean value is located. The horizontal lines correspond to measured values, and the vertical lines to the simulated values. The horizontal lines are equal because the same data has been used in both simulations.

In Figure 4.3 the data from Table 4.1 have been used to create a least-square approximation. For each simulation a straight line has been fitted with the measured mean values as a function of the simulated mean values.

4.1.2 Extending the Comparison to More Data

To even more eliminate the possibilities that the parameter settings causes that the simulated ionization peak is a few CAD early, a comparison of more data has been made. The simulations have been done with four different lambda values and compared to the corresponding measured data and are presented in Table 4.2.

4.1.3 Results of the Sensitivity Analysis

The last step in the first part is a sensitivity analysis. Here all the simulation and engine parameters are increased and decreased by ten percent. For each parameter set a simulation has been run. If the
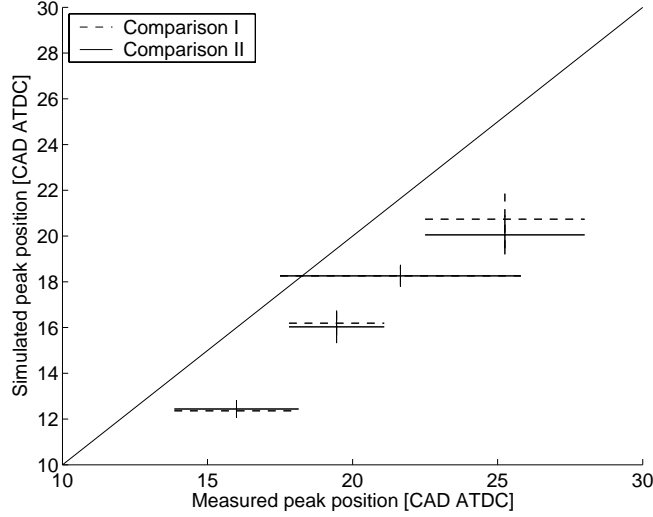
Figure 4.2: *The simulated position of the ionization peaks against the measured peaks. The length of the lines is two standard deviations, and the mean value is the middle of the line. The large standard deviations in the measured data are a consequence of the large cycle-to-cycle variations in the measured ionization current data. Another consequence is that the measured data is quite noisy which makes it hard to determine the correct peak position. As can be seen the data from the two simulations are almost identical. Comparison I was done by Nogenmyr and comparison II was done in this thesis.*

	Comparison III		Measured	
λ	Mean	Std	Mean	Std
0.8824	11.17	0.44	13.25	1.67
0.9200	11.46	0.62	14.00	2.88
0.9536	12.32	0.50	15.00	1.41
1.0682	14.50	0.75	18.40	0.55

Table 4.2: *Mean values and standard deviations of the ionization peaks. The simulations have been done with four different lambda values and $\theta_0 = 27.2$. The simulated peaks are still 2–4 CAD earlier then the measured peaks.*
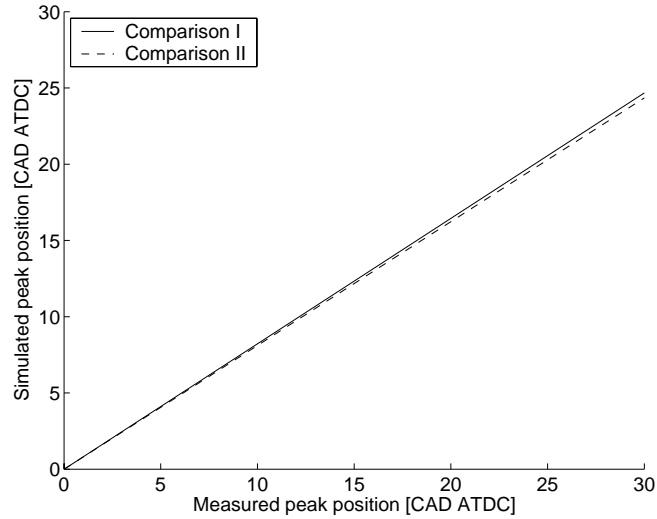
Figure 4.3: *A least-square approximation of the mean value data from Table 4.1. As can be seen in the plot the approximations from the two different fittings are almost identical. Comparison I was done by Nogenmyr and comparison II was done in this thesis.*
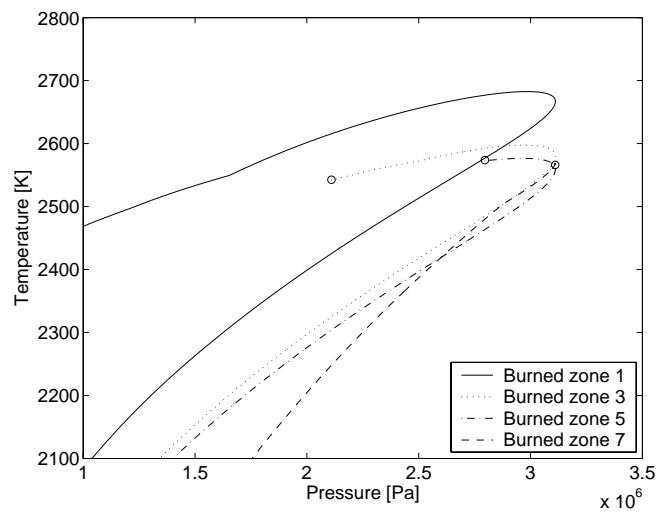
Figure 4.4: *The temperature of four different zones plotted as functions of the pressure of the zone. The numbering of the zones is explained in Figure 4.5.*
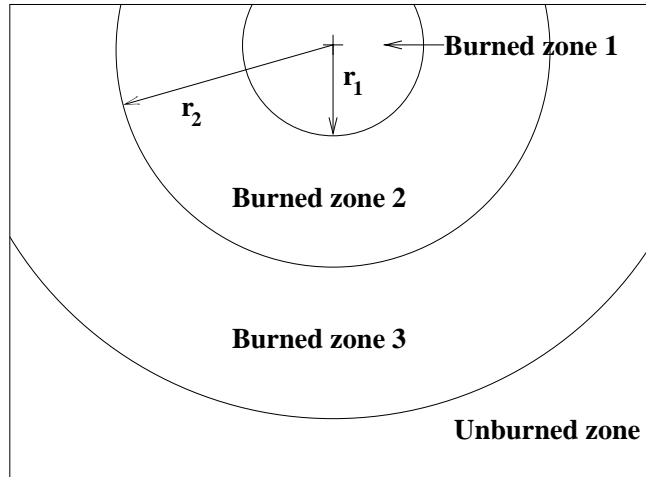
Figure 4.5: *This shows the shells in a typical situation.*
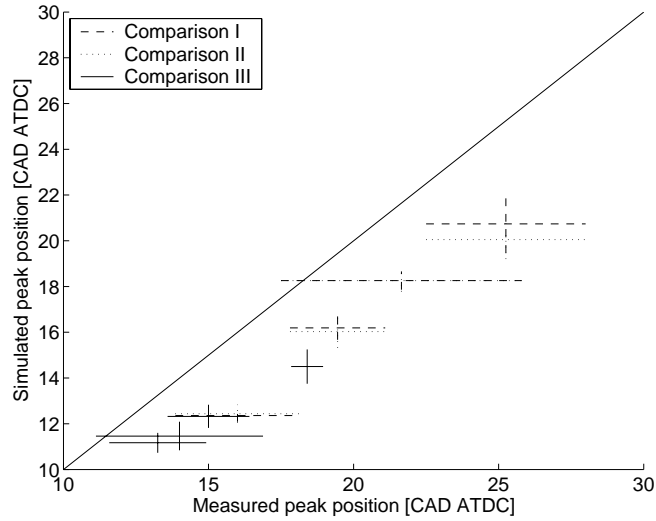
Figure 4.6: *Comparison III done with four different lambda values. The length of the lines is two standard deviations, and the mean value is located in the middle of the line. Comparison I was done by Nogenmyr and comparison II was done in this thesis.*

| Parameter	Value	-10%	$+10\%$	Ranking
$WoschniC_1$	2	-0.44	0.47	1
$WoschniC_2$	0.44	-0.18	0.33	2
t_{Stop}	0.0736	≈ 0	≈ 0	4
m	4	0.46	-0.32	1
a	20	0.34	≈ 0	2
p_{ivc}	6.5e4	0.18	≈ 0	3
T_{ivc}	363	≈ 0	0.23	2
ϕ	1	≈ 0	≈ 0	4
ϕ_{res}	1	≈ 0	≈ 0	4
x_{res}	0.065	0.11	≈ 0	3
Lst	14.7	≈ 0	≈ 0	4
$initBurnedVolFrac$	1e-5	0.11	≈ 0	3
$massLimit$	4.7e-5	≈ 0	≈ 0	4
$FlameSpeed$	4.5	≈ 0	≈ 0	4

Table 4.3: *Simulation data from the sensitivity analysis. The simulation parameters have been decreased and increased by ten percent.*

simulation did not converge the parameter change was decreased to one percent.

The results are presented in the Tables 4.3, 4.4, 4.5 and 4.6. The values presented in the table are calculated by first taking the distance between the pressure peak and ionization peak without any parameter change. Then the distance between the pressure peak and ionization peak in simulation data with a parameter change was calculated. These two values are then subtracted from each other.

As can be seen in Table 4.3 and 4.4, all the values are under a half degree. This means that a small parameter change has little influence on the result. Even in Table 4.5 and 4.6 the values are small, except for θ_s and θ_E. But a change of one percent in these parameters are not realistic, because the θ_s and θ_E parameters are converted to simulation time. Then a one percent increase or decrease of that time value becomes very big.

In Table 4.7 and 4.8 gives an short explanation of all the parameters used in the sensitivity analysis.

Parameter	Value	-10%	$+10\%$	Ranking
a	3.9e-2	0.34	≈ 0	1
l	15.9e-2	≈ 0	≈ 0	2
V_d	4.96e-4	-0.18	0.33	1
dt	2e-3	≈ 0	≈ 0	3

Table 4.4: *Simulation data from the sensitivity analysis. The engine parameters have been decreased and increased by ten percent.*

Parameter	Value	-1%	$+1\%$	Ranking
T_{wall}	470	≈ 0	0.11	3
ω	200	≈ 0	≈ 0	4
t_{Start}	0.0497	≈ 0	≈ 0	4
θ_S	12.09	0.98	-0.89	1
θ_E	13.33	-0.45	0.67	2
η	0.99	≈ 0	≈ 0	4
h	2e-5	≈ 0	≈ 0	4

Table 4.5: *Simulation data from the sensitivity analysis. The simulation parameters have been decreased and increased by one percent.*

Parameter	Value	-1%	$+1\%$	Ranking
B	9.0e-2	≈ 0	0.11	3
r_c	9.25	≈ 0	≈ 0	4
V_c	6.01e-5	≈ 0	0.10	4
S	0.078	≈ 0	≈ 0	4

Table 4.6: *Simulation data from the sensitivity analysis. The engine parameters have been decreased and increased by one percent.*

T_{wall}	Temperature at the cylinder wall [K]
$WoschniC_1$	Heat transfer constant [ ]
$WoschniC_2$	Heat transfer constant [ ]
ω	The angular velocity [rad/s]
t_{Start}	Simulation start-time [s]
t_{Stop}	Simulation stop-time [s]
θ_S	Start of combustion [CAD]
θ_E	Combustion duration [CAD]
η	Parameter in the Vibe function [ ]
m	The m parameter for the Vibe function [ ]
a	The a parameter for the Vibe function [ ]
p_{ivc}	Pressure at intake valve close [Pa]
T_{ivc}	Temperature at intake valve close [K]
phi	Fuel / air equivalence ratio [ ]
phi_{res}	Fuel / air equivalence ratio in residual gas [ ]
x_{res}	Residual gas fraction [ ]
Lst	Stoichiometric air/fuel ratio [ ]
h	The timestep of the simulation [s]
$initBurnedVolFrac$	Fraction in the unburned zone used to create a burned zone [ ]
$massLimit$	The maximum mass that a boundary zone might have [kg]
$FlameSpeed$	The speed of the flame [m/s]

Table 4.7: *Simulation parameters that were increased and decreased in the sensitivity analysis. A short explanation to each parameter is also given.*

a	Crank radius [m]
l	Connecting rod length [m]
B	Cylinder bore [m]
r_c	Compression ratio [ ]
V_d	Displaced volume [m^3]
V_c	Clearance volume [m^3]
S	Piston stroke [m]
dt	Distance spark-gap to cylinder head [m]

Table 4.8: *Engine parameters that were increased and decreased in the sensitivity analysis. A short explanation to each parameter is also given.*
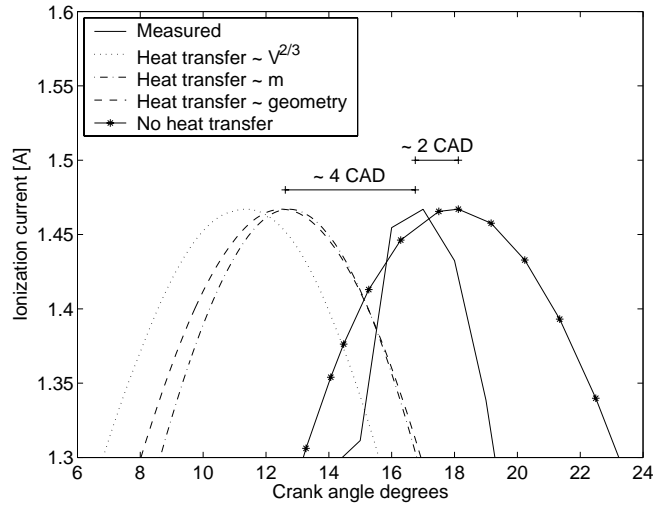
Figure 4.7: *Simulations done with different heat transfer models and without heat transfer. The data is compared to the measured data. It can be seen that simulations with heat transfer results in a ionization current peak location about 4 CAD earlier than the measured peak location. But simulations without heat transfer results in a ionization current peak location about 2 CAD later than the measured peak location. The first observation was done by Karl-Johan Nogenmyr in [9] and has been analyzed in this thesis. The second observation was done by Ingemar Andersson in [2].*

4.2   Comparison with Other Models

In Figure 4.7 the difference between the simulated peak location with heat transfer and without heat transfer, can be seen. When Andersson did his simulations he did not include heat transfer. The ionization current peak is located about 2 CAD later than the measured. But by including heat transfer the peak location is moved to a position 4 CAD earlier than the measured peak.

Figure 4.8 shows the results from simulations done with 1–14 burned zones. The value of the y-axis is the ionization peak position, which is quite stabile for simulations done with 2–14 burned zones. The reason that the simlation done with one burned zone differs, is that the spark plug is located in the first burned zone, and the heat transfer with that zone is quite big. In Figure 4.9 the ionization current peak location
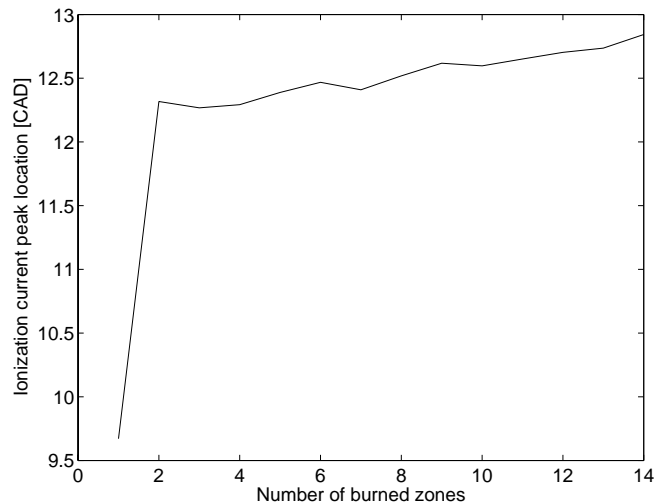
Figure 4.8: *The ionization current peak location for simulations done with different number of zones. The low value for the simulation done with one zone depends on the large heat transfer, which is a consequence of the geometry.*

has been plotted for simulations done with three different massflows between the zones. The difference between the three simulations is very small, about 0.1 CAD.

4.3   Improved Model Agreement

4.3.1   Including a Dynamical NO-Model

Section 4.1 showed that the static NO-model did not explain all the dynamics in ionization current formation. Therefore an extension of the model with a dynamical NO-model was considered. In [2], simulation with a two-zone model and dynamical NO-model shows that the ionization current peak occurs about 2 CAD later than simulations done with a static NO-model. The expectation is that the same peak delay occurs even in the multi-zonal model using dynamical NO. In Table 4.9 the results from the simulations with dynamical NO are presented. It can be seen that the dynamical NO-model give rise to a delay in the ionization current peak, even in the multi-zonal model. A comparison between Table 4.1 and 4.9 shows that the peak delay is about 3–4 CAD. The simulated- and measured ionization currents peak position in Table 4.9 are within 1 CAD, and the standard deviations for the simulated curves are approximately 1 CAD.
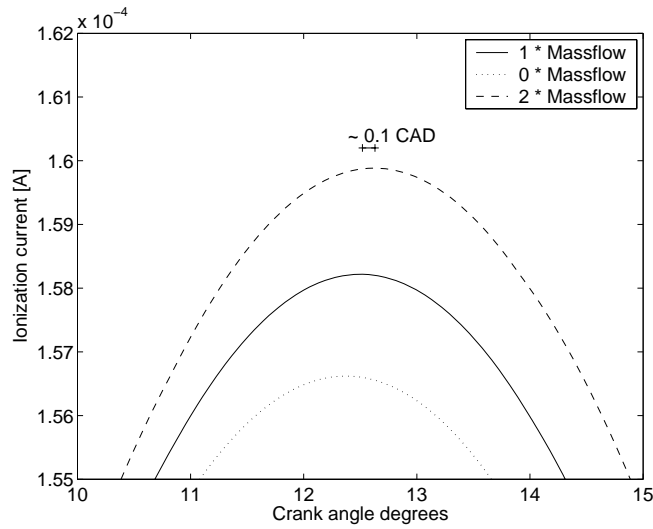
Figure 4.9: *The ionization currents plotted for different massflow between the zones. The difference between the three simulations is very small, about 0.1 CAD.*

θ_0 [CAD BTDC]	Comparison		Measured	
	Mean	Std	Mean	Std
27.0	16.67	0.70	16.00	2.14
24.1	18.75	0.86	19.45	1.64
21.1	21.25	1.12	21.65	4.15
18.1	24.41	0.69	25.25	2.75

Table 4.9: *Data from simulations done with the dynamical NO-model. Now the simulated and measured peak positions of the ionization currents are within 1 CAD. The standard deviations from the simulations are approximately 1 CAD.*

(a) Ignition angle 27.0 CAD BTDC

(b) Ignition angle 24.1 CAD BTDC

(c) Ignition angle 21.1 CAD BTDC

(d) Ignition angel 18.1 CAD BTDC
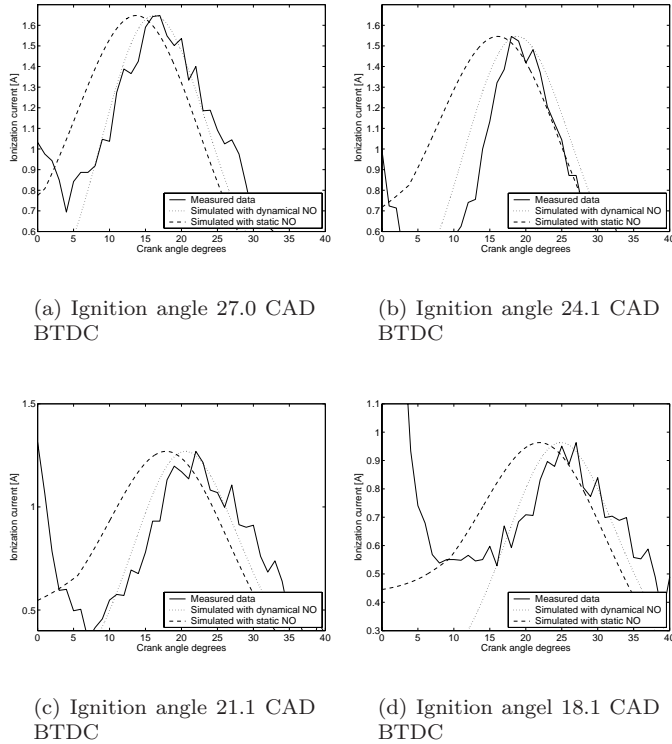
Figure 4.10: *The measured- and simulated ionization current for four different ignition angles are plotted. The plot with dynamical NO shows good agreement with the measured plot. Simulation parameters can be found in Appendix A.3.*

In Figure 4.10 the ionization currents have been plotted for four different ignition angles. The amplitudes of the curves are normalized.

In Figure 4.11 the equilibrium and dynamical NO concentrations are plotted. Figure 4.11(a) shows the concentrations for the first burned zone, Figure 4.11(b) for the third burned zone, Figure 4.11(c) for the fifth burned zone and Figure 4.11(d) for the seventh burned zone.

(a) Burned zone 1

(b) Burned zone 3

(c) Burned zone 5
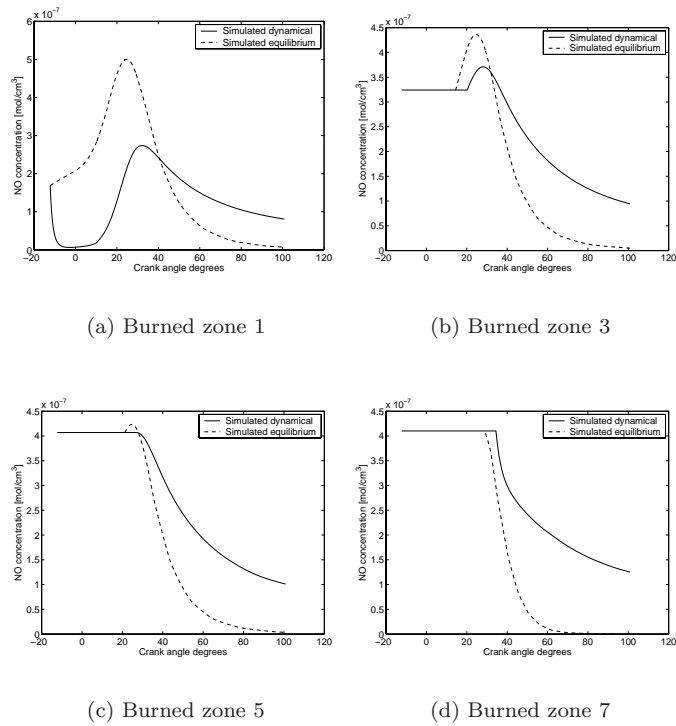
(d) Burned zone 7

Figure 4.11: *Equilibrium and dynamical NO concentration for the first- and second burned zone. The equilibrium concentrations are calculated using CHEPP. Simulation parameters can be found in Appendix A.1.2.*
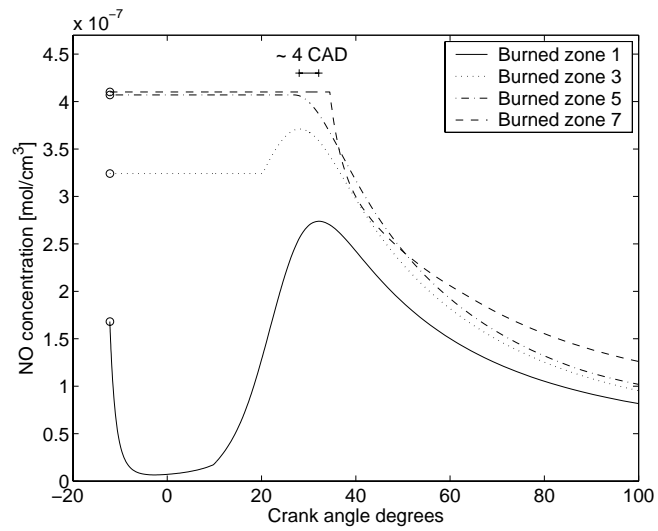
**Figure 4.12:** *Simulated NO concentration for burned zones 1, 3, 5, 7 using dynamical NO.*
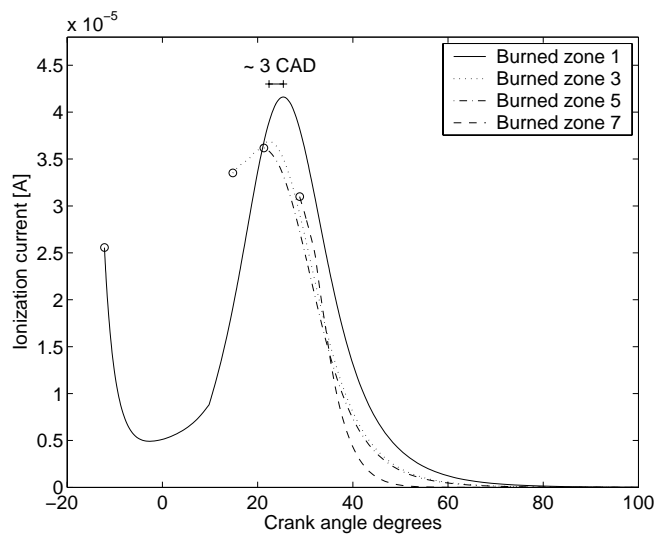
Figure 4.13: *Simulated ionization currents for burned zones 1, 3, 5, 7 using dynamical NO.*

Chapter 5

Conclusions and Future Work

5.1 Conclusions

The purpose of this thesis was to give answer to the three points stated in the introduction.

1. When doing simulations with the multi-zonal, static NO and heat transfer model, the observation that the simulated ionization current peak location always is a few CAD earlier than the measured peak, seems to be correct. Repeating the simulations Karl-Johan Nogenmyr did in his thesis leads to almost the same ionization peak locations. This means that the model is not very sensitive in the two different manually made pressure curve fittings. The fittings was also extended with more data, but the results showed even here that the ionization current peak location was about 2–4 CAD to early. At last the sensitivity analysis showed that almost all parameters had none or very small influence on the results. In Figure 5.1 the ionization current curve has been plotted for one cycle at a certain working point. The curve corresponding to all this above is the curve marked *Heat transfer - geometry*. It can clearly be seen that the simulated curve is located a few CAD to early. Even other heat transfer models have been used and the results have been plotted in Figure 5.1.

2. An explanation of the difference between Karl-Johan Nogenmyr's and Ingemar Andersson's results is that Nogenmyr included heat transfer in his model, which Andersson did not. This heat transfer makes the ionization current peak moving about 8 CAD earlier. In Nogenmyr's model there is also included a massflow between
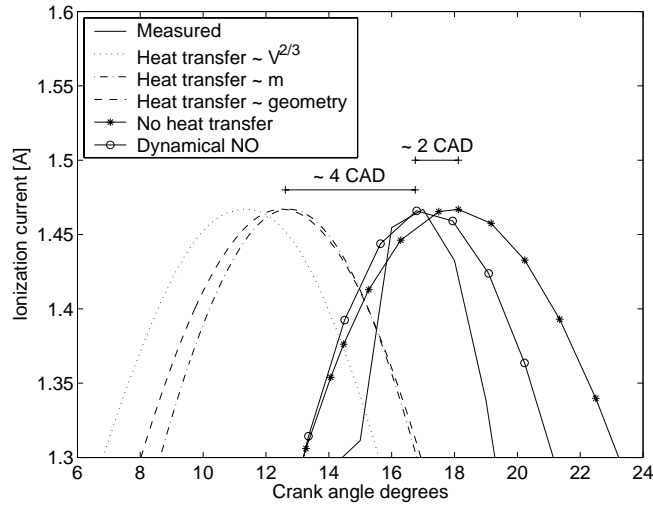
Figure 5.1: *Here ioinization current curves for all the different models are plotted. It can be seen that the peak from the model without heat transfer is located about 2 CAD later than the measured peak. The peak for the models with heat transfer is located about 4–5 CAD earlier than the measured peak. For the latest model with heat transfer and dynamical NO, the peak is located within 1 CAD from the measured peak.*

the zones. But this massflow has very little influence on the peak location. This can be seen in Figure 4.9. Another explanation is the multi-zonal model. In Figure 4.8, it can be seen that simulations done with only one burned zone differs quite much from simulations done with more zones. This would move the peak location about 2 CAD later than Andersson's who used only one burned zone.

3. After the implementation of a dynamical NO-model, the simulated and measured ionization current peak locations are within 1 CAD. The result is within the margin of error. Trying to achieve better agreement is not relevant, because of the noise in the measured data. Figure 5.1 shows the ionization current curve, using the dynamical NO-model.

5.2 Future Work

- Making the Java program easier to use with a Graphical User Interface (GUI).

- Invert the fitting. First do simulations, and then use the results to predict the pressure peak location.

- Investigate why the measured absolute value of the ionization current differs so much from the simulated value.

References

[1] T. Berglind A. Saitzkoff, R.Reinmann and M. Glavmo. An ionization equilibrium analysis of the spark plug as an ionization sensor. 1996. SAE paper no. 960337.

[2] I. Andersson. *Cylinder Pressure and Current Modeling for Spark Ignited Engines.* Thesis no. 962, Department of Electrical Engineering, Linköpings Universitet, Linköping, Sweden, May 2002.

[3] Lars Eriksson. Thermodynamics of unsteady flows and zero dimensional in-cylinder models, October 2002.

[4] Lars Eriksson. Chepp – a chemical equilibrium program package for matlab. Technical report, 2004. SAE 2004-01-1460.

[5] Lars Eriksson and Lars Nielsen. Towards on-board engine calibration with feedback control incorporating combustion models and ion-sense. *at – Automatisierungstechnik*, 51(5):204–212, 2003.

[6] Johan Gill. A Java Package for Simulation of Combustion Engines. Master's thesis LiTH-ISY-EX-3342-2003, Linköping University, SE-581 83 Linköping, 2003.

[7] John B. Heywood. *Internal Combustion Engine Fundamentals.* McGraw-Hill series in mechanical engineering. McGraw-Hill, 1992.

[8] Ylva Nilsson and Lars Eriksson. A New Formulation of Multi-Zone Combustion Engine Models. Karlsruhe, Germany, IFAC Workshop: Advances in Automotive Control, 2001.

[9] Karl-Johan Nogenmyr. Development and Analysis of Zonal Models for a Combustion Engine. Master's thesis LiTH-IFM-Ex-Fysik-1110, Linköping University, SE-581 83 Linköping, 2003.

[10] C.R Ferguson R.J. Tabaczunski and K Radhakrishnan. A turbulent entrainment model for a spark-ignition engine combustion. 1977. SAE 770647.

[11] R.J. Tabaczunski S.D. Hires and J.M. Novack. The prediction of ignition delay and combustion intervals for a homogeneous charge, spark ignition engine. 1978. SAE 780232.

[12] G. Woschni. Universally Applicable Equation for the Instantaneous Heat Transfer Coefficient in the Internal Combustion Engine. 1967. SAE paper 670931.

Notation

Symbols used in the report.

Variables and parameters

NO	Nitrogen oxide
N_2	Nitrogen
O_2	Oxygen
OH	Hydrogen oxide
O	Oxygen
N	Nitrogen
T	Temperature [K]
p	Pressure [Pa]
ϕ	Normalized fuel/air equivalence ratio [ ]

Abbreviations

CAD	Crank Angle Degrees
TDC	Top Dead Center, engine crank position at 0 CAD
ATDC	After TDC
BTDC	Before TDC
IVC	Inlet Valve Close
ϕ	Fuel/air equivalence ratio
Lst	Stoichiometric fuel/air ratio
DIRK	Diagonally Implicit Runge-Kutta Integrator
CHEPP	CHemical Equilibrium Program Package, a MATLAB based software package for calculating chemical equilibrium concentrations in a gas mixture.
ODE	Ordinary Differential Equation
GUI	Graphical User Interface

Appendix A

Measurement Background

A.1 Parameters in the Java Implementation

A.1.1 Engine parameters

Crank radius	39 [mm]
Connecting rod	159 [mm]
Bore	90 [mm]
Compression ratio	10:1 [ ]
Displacement volume	4.94e-4 [m^3]
Clearence volume	5.99e-5 [m^3]
Stroke	78 [mm]
Distance spark-gap to cylinder head	2 [mm]

A.1.2   Simulation Parameters

Cylinder wall temperature	470 [K]
Woschni C_1	1 [ ]
Woschni C_2	1/2.28 [ ]
Crank angular velocity	200 [rad/s]
Intake valve close	125 [CAD BTDC]
Exhaust valve open	123 [CAD ATDC]
Ignition angle	27.0 [CAD BTDC]
Combustion duration	44 [CAD]
Vibe η parameter	0.99 [ ]
Vibe m parameter	2 [ ]
Vibe a parameter	20 [ ]
Pressure @ IVC	65 [kPa]
Temperature @ IVC	363 [K]
ϕ	1 [ ]
ϕ_{res}	1 [ ]
Residual gases	0.065 [ ]
κ	1.4 [ ]
Lst	14.7 [ ]
Time step in simulation	2e-5 [s]
Smallest mean step length	1e-7 [ ]
Maximum time step	8e-5 [s]
DIRK error parameter	1e-5 [ ]
Jacobian absolute pertubation parameter	1e-12 [ ]
Jacobian relative pertubation parameter	1e-4 [ ]
Initial volume of a burned zone	1e-5 [m^3]
Maximum zone mass	4.7e-5 [kg]
Heat transfer type	Calculated from geometry
Combusted part	0.97 [ ]

A.2   Parameters in the Dynamical Java Implementation

ϕ	1.0 [ ]
Simlation time step	1e-12 [s]
Absolute error	1e-13 [ ]
Relative error	1e-6 [ ]
Integrator type	Runge-Kutta Pair

A.3   Parameters used in the fittings

Ignition angle	27.0	24.1	21.1	18.1
Combustion duration	47	49	49	54
Temperature @ IVC	360	368	368	368
Residual gases	0.060	0.065	0.065	0.065

Appendix B

A short `NOSimulator` manual

The program consist of several class files. The `NOSimulator.java` file handles the simulator and its parameters. It also handles the writing of data to file. Data is written as a big matrix.

- Column 1 corresponds to the crank angle.

- The second column is the ionization current for the first burned zone.

- Column number 3 – 9 are the dynamical NO concentration for all the burned zones in order 1 – 7.

- Column 10 to 15 are the ionization current for burned zone 2 – 7.

- Column 16 – 20 are the equilibrium NO concentration for burned zone 1, 2, 3, 5, 7.

Output data is saved in the file `outData_NO.dat`.

Listed below are some of the parameters for the integrator.

```
ExtendedButcherTable table =
    ExtendedButcherTable.
        getExtendedButcherTable("RKF(4,5)");

TimeContinuous f = new NOModel(phi);

double t = (((NOModel)f).
    getZoneStartTime(1) +
        0.0005); //Simulation start time
```

```
double h = 1e-12; //Timestep
double epsa = 1e-13; //Absolute error
double epsr = 1e-6; //Relative error

Integrator integrator =
    new RungeKuttaPairIntegrator(table,
        f, t, h, epsa, epsr);
```

The `NOModel.java` file contains the entire dynamical NO model. All the equilibrium data comes from CHEPP [4] and are converted into java objects with the program `EqDataReader.java`. These objects are then used in the simulation program.

To start the program first compile it with the commando

```
javac -classpath Janet.jar:. *.java
```

then to start the simulation

```
java -classpath Janet.jar:. NOSimulator
```

The program reads the file `outData.dat` which must be on the form

- Simulation time in column 1.

- The spark plug zone in column 2.

- Pressure in column 3

- The remaining columns should consist of volume and temperature for each zone.

Copyright

Svenska

Detta dokument hålls tillgängligt på Internet - eller dess framtida ersättare - under en längre tid från publiceringsdatum under förutsättning att inga extra-ordinära omständigheter uppstår.

Tillgång till dokumentet innebär tillstånd för var och en att läsa, ladda ner, skriva ut enstaka kopior för enskilt bruk och att använda det oförändrat för ickekommersiell forskning och för undervisning. Överföring av upphovsrätten vid en senare tidpunkt kan inte upphäva detta tillstånd. All annan användning av dokumentet kräver upphovsmannens medgivande. För att garantera äktheten, säkerheten och tillgängligheten finns det lösningar av teknisk och administrativ art.

Upphovsmannens ideella rätt innefattar rätt att bli nämnd som upphovsman i den omfattning som god sed kräver vid användning av dokumentet på ovan beskrivna sätt samt skydd mot att dokumentet ändras eller presenteras i sådan form eller i sådant sammanhang som är kränkande för upphovsmannens litterära eller konstnärliga anseende eller egenart.

För ytterligare information om Linköping University Electronic Press se förlagets hemsida: `http://www.ep.liu.se/`

English

The publishers will keep this document online on the Internet - or its possible replacement - for a considerable time from the date of publication barring exceptional circumstances.

The online availability of the document implies a permanent permission for anyone to read, to download, to print out single copies for your own use and to use it unchanged for any non-commercial research and educational purpose. Subsequent transfers of copyright cannot revoke this permission. All other uses of the document are conditional on the consent of the copyright owner. The publisher has taken technical and administrative measures to assure authenticity, security and accessibility.

According to intellectual property law the author has the right to be mentioned when his/her work is accessed as described above and to be protected against infringement.

For additional information about the Linköping University Electronic Press and its procedures for publication and for assurance of document integrity, please refer to its WWW home page: `http://www.ep.liu.se/`